International Journal of Computer Information Systems and Industrial Management Applications
ISSN 2150-7988 Volume 18(16s) 2026 pp. 1275-1294
https://doi.org/10.70917/ijcisim-2026-4657
Article

Estimation of Battery charging for Electric vehicle using soft computing techniques

S.Arulkumar[1], K.E.Lakshmiprabha[2], P.Rajivgandhi[3], M.Saravanan[4]

[1]Department of Electrical and Electronics Engineering, Academy of Maritime Education and Training (AMET), Deemed to be University, Chennai, India.
Corresponding Author: arulkumar.eee2004@ametuniv.ac.in
[2]Department of Electrical and Electronics Engineering, Karpaga Vinayaga College of Engineering and Technology, KVELL (Deemed to be University), Chengalpattu, India.
[3]Department of Electrical and Electronics Engineering, Adhiparasakthi Engineering College, Melmaruvathur, India.
4Department of Electrical and Electronics Engineering, Holymary Institute of Technology and Sceince, Hyderabad, India.

Abstract: The objective of this work is to estimate the SOC in Lithium-Ion batteries used in electric vehicles (EVs). The generalized linear model (GLM) is applied, the GLM method with Poisson regression and a linear interpolation in estimating the SOC. The coefficient of the models is obtained from three machine learning techniques. The new SOC estimation strategies are tested applied to a Lithium battery model computationally implemented in four driving profiles and comparison of the results obtained between the proposed method and other existing methods in the literature are performed.
Keywords: State of charge, Electric vehicle, Lithium-ion battery, Machine learning techniques

1. Introduction

The global electricity sector undergoes few technological changes in the face of all the advances that occurred in the 20th century, and this scenario has changed in the last decade with the advent of the concept of Intelligent Electric Networks (smart grids), which is based on the use of technologies of communication and information with a view to providing monitoring, control and insertion of new technologies in the electrical grid, which have changed society's interaction with the energy sector [1-8].

In this way, the search for solutions to preserve the planet Earth for future generations necessarily involves the design of electrical grids that favor the reduction of atmospheric pollution. In this context, electrical grids propelled by sustainable energy sources are the central theme. Not by chance, the main manufacturers in the world have been researching and developing electrical grids that use alternative energy sources and several countries have already announced goals to reduce the problem: Germany has committed to banishing electrical grids powered by fossil fuels by 2030, England will stop the sale of new electrical grids powered by oil derivatives from 2040 and, in Norway and India, only fully electrical grids will be marketed from 2015 and 2030, respectively [9-13].

The search for sustainable energy sources to equip electrical grid has led researchers to investigate everything from solar energy and compressed gases to fuels based on algae and alcohol. Among the emerging technologies are electrical grids [14-19] and those powered by hydrogen. The main car manufacturers already have commercial versions of electrical grids of this type, although their establishment as a real successor to the current ones and their use on a large scale still require a lot of research and development.

Another widespread classification divides electrical grids into load maintainers or depletors. The first ones are capable of keeping the battery charge within determined limits in any driving situation, and the others do not have this capacity and need to be connected to the electrical network periodically to recharge the battery.

The use of different energy sources in the same car requires a power management strategy that divides the power demand between the sources and gives the electrical grid adequate performance [20-24]. The power management strategy can be performed using different approaches, grouped into three categories, namely: Heuristic techniques; Static optimization methods and Dynamic optimization methods. Heuristic techniques are well explored in the literature [25-29] and have in their favor the ease and low cost of implementation, although they generally do not fully explore complex grids. In static optimization methods the electrical power is translated into an equivalent amount of steady state fuel consumption to calculate the total cost. An optimal control strategy then determines the appropriate division of the power demand between each of the sources, using efficiency maps. Therefore, they are methods of instantaneous optimization according to the system variables at each instant of time. The most widespread method of this class is called Equivalent Consumption Minimization Strategy (ECMS). The dynamic optimization methods consider the dynamics of the system and the optimization starts to be considered according to a time horizon, instead of specific instants. Although it has global optimization capability, these methods have the disadvantages of being dependent on the driving cycle and cannot be implemented in real time. An application example is found in [30] and [32], where the energy management (EM) for a hybrid truck with parallel configuration is done. In order to enhance energy management and economic performance, recent research has suggested sophisticated optimization strategies for community microgrids that include EVs, ESSs, and PV systems. An IoT-based smart metering framework for solar PV-powered EV charging stations is developed using IRSA-SHA for secure communication and MSSA for route optimization. By outperforming ACO and TAC algorithms and achieving high packet delivery, low latency, and improved network stability, the proposed approach facilitates sustainable EV charging applications [33]. A CNN-based battery management system with a SEPIC converter is developed for efficient EV charging and V2G operations. The converter switches between buck and boost modes based on battery SOC, and a PI controller regulates grid power exchange. The proposed method improves energy efficiency, system reliability, and grid stability [34].

2. METHODOLOGY PROCEDURES

This section discusses the methodological procedures used in order to achieve the objectives defined for the present study, as well as presenting the models and justifications for their use.

2.1 DATABASE

The battery used to carry out this study was the INR 18650-20R Li NiMnCoO2/Graphite, which has a nominal voltage of 3.6V, nominal capacity of 2000mAh, minimum voltage of 2.5V, maximum voltage of 4.2V, maximum current from 22A to 25∘C and an operating temperature ranging from 0∘C to 50∘C.

The tests take place in three controlled temperature ranges so that the SOC can be determined by the Ah method within the battery operating range, namely: 0ºC, 25ºC and 45ºC with the initial SOC at 50% and 80%.

2.2 MODEL TRAINING

For training the models discussed in the previous section, the initial capacity curve was used. Through this test, various information about the behavior of the battery can be obtained. As the temperature values are controlled, the SOC values can be obtained using the Ah method.

Figure 1 presents the initial capability curve used for training all models. Obtaining the mathematical equation that represents this curve is done offline and, once this equation is obtained, it can be loaded into the BMS45 to carry out the SOC forecast online.

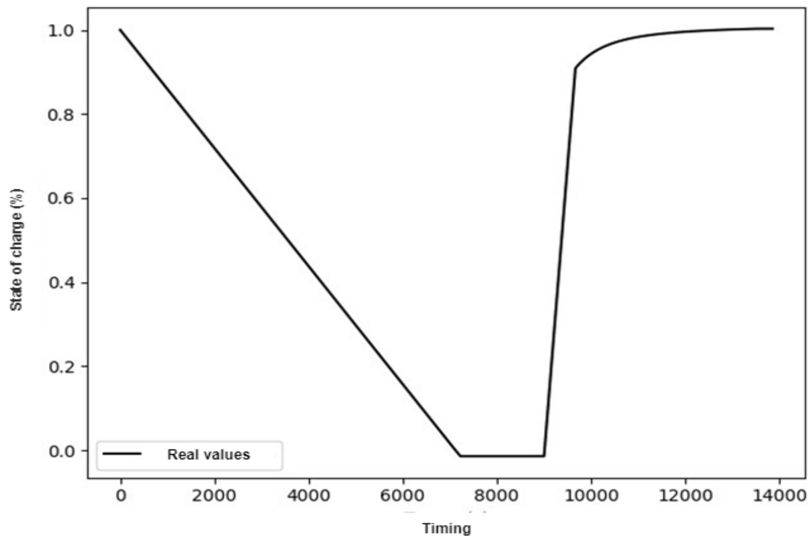

Figure 1 – Initial Capacity curve

Figure 2 shows the I-V curves obtained from the initial capacitance test.

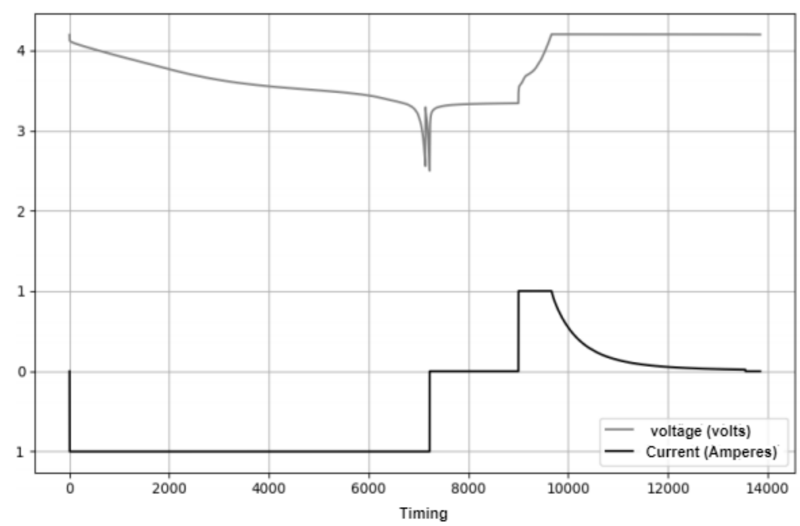

Figure 2 - Voltage and Current Profile of the Initial Capacity Test

2.3 EVALUATION METRICS

Absolute Error (AE) was used as an objective function or performance evaluation metric, as shown in Equation 1.

$$AE = \sum_{t=1}^{N} \quad |d_t - y_t| \tag{1}$$

Such that, N is the samples, dt is the SOC, and yt is the predicted by one of the linear models.

Another metric used is the Mean Square Error, from the English Mean Square Error (MSE), according to Equation 2, which is widely used in the literature because it features a greater penalty for larger errors, which, consequently, have a greater influence on the final value of the forecast, and a smaller penalty for the model that presents smaller errors:

$$MSE = \frac{1}{N}\sum_{t=1}^{N} \quad (d_t - y_t)^2$$

(2)

And finally, the last metric used is the Mean Absolute Error (MAE), shown in Equation 3.

$$MAE = \frac{1}{N}\sum_{t=1}^{N} \quad |d_t - y_t|$$

(3)

2.4 FORECASTING MODELS APPROACHED

In this work, 3 linear models were considered, GLM, POISSON, and SPLINE, combined with three different optimization techniques: GA, DE, and PSO called GLM-GA (I), GLM-DE (II), GLM-PSO (III), POISSON-GA (IV), POISSON-DE (V), POISSON-PSO (VI), SPLINE-GA (VII), SPLINE-DE (VIII), and SPLINE-PSO (IX). These techniques aim to perform the adjustment of the respective coefficients of each model, totaling 9 implemented variations. The objective function used was the Absolute Error, shown in Equation 8. No restrictions were used to perform the tests.

The models were implemented in Python. It has a wide range of modeling capabilities, including renewable energy sources, energy storage systems, and power electronics.In order to obtain a statistical sampling of performance, each algorithm was executed 50 times, so that the best execution was chosen, that is, the configuration that presented the smallest AE was selected. The configuration used in each model is:

2.5 **MODEL TESTING**

The four tests occur from 80 percent and 50 percent of initial SOC until the final value of 10% of SOC, these state of charge values are used because it is in this range of SOC that the operation in an EV occurs.

2.5.1 URBAN TEST DRIVING

FUDS profile was based on the urban driving test standard established by the automobile industry.Each cycle of this complex test profile is 1372 seconds long and was originally inspired by data obtained through real driving. The initial and final SOC conditions are the same as the DST test profile.

Figure 3 presents the complete test profile, where in black we have the current profile in Amps and in gray we have the voltage profile in Volts. Negative current means the battery is being discharged and +ve current means the battery is being charged.

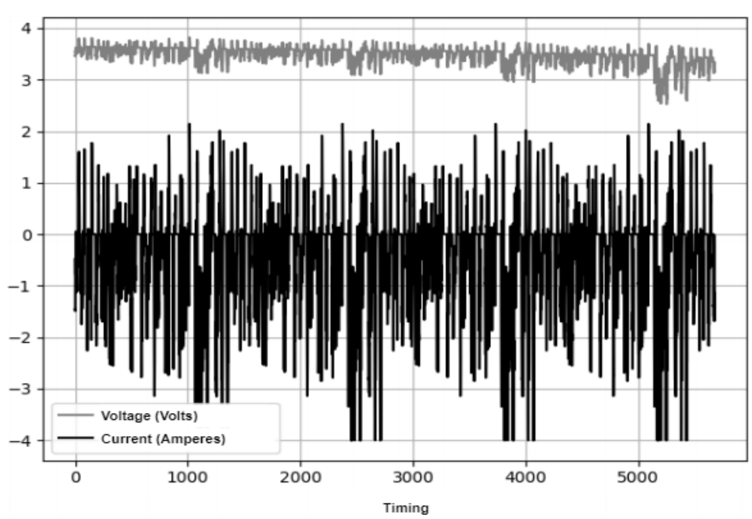

Figure 3 - Voltage and Current Curve FUDS test profile

2.5.2 DYNAMIC STRESS TESTING (DST)

The DST profile has a 360 second cycle that is repeated until the discharge end point is based on the net capacity removed. This net capacity refers to the difference between the energy injected into the battery and the energy removed from the battery.

Figure 4 presents the complete test profile, where in black we have the current profile in Amps and in gray we have the voltage profile in Volts. -ve current means the battery is being discharged and +ve current means the battery is being charged.

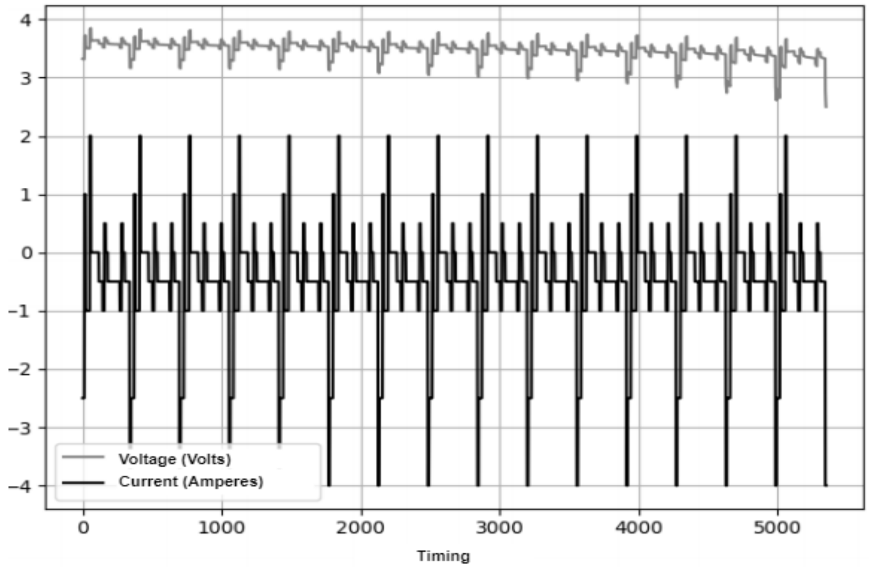

Figure 4 – Voltage and Current Curve DST Test Profile

2.5.3 HIGHWAY DRIVING TEST

A cycle of the US06 is 600 seconds long and represents an aggressive test drive performed on a highway (max. speed ~ 129.2 km/h, max. acceleration ~ 3.2 m/s2). The initial and final SOC conditions are the same as in the DST test profile.

Figure 5 shows the complete test profile, where in black we have the current profile in Amperes and in gray we have the voltage profile in Volts. -ve current means the battery is being discharged and +ve current means the battery is being charged.

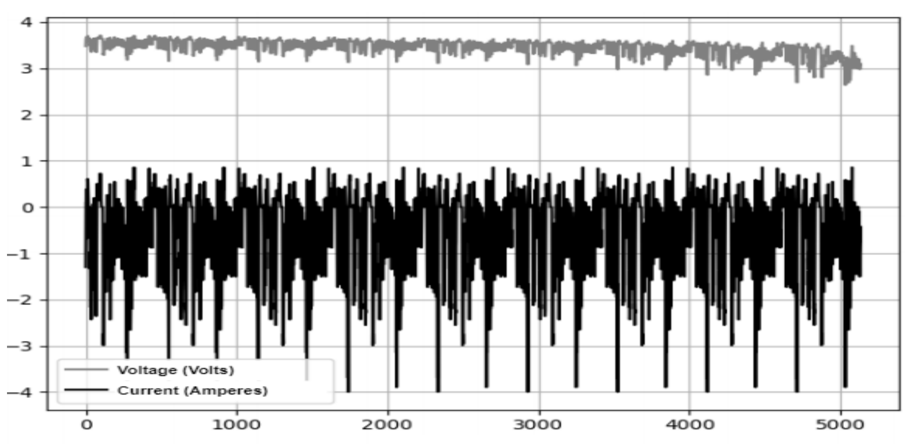

Figure 5 - Voltage and Current Curve Test Profile US06

2.5.4 BEIJING DYNAMIC TEST

The BJDST test profile indicates a wealth of information about EV operating and utilization patterns comprising acceleration, velocity, and deceleration among others. Each BJDST cycle is 916 seconds long. The initial and final SOC conditions are the same as the DST test profile.

Figure 6 presents the complete test profile, where in black we have the current profile in Amps and in gray we have the voltage profile in Volts. -ve current means the battery is being discharged and +ve current means the battery is being charged.

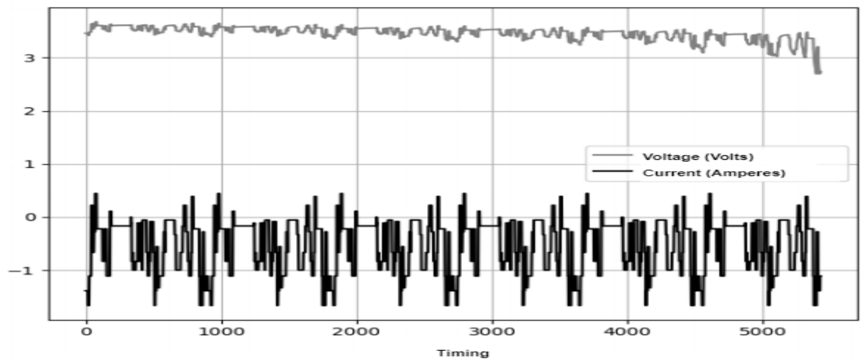

Figure 6 – Voltage and Current Curve BJDST Test Profile

This section addressed the methodological procedures employed in carrying out this study. In which, initially, the database used to carry out the predictions was presented and the calibration methodology of the models was defined, which was obtained through training under the initial battery capacity curve.

Performance evaluation metrics were presented, which are used by the optimization algorithms as a cost function in the model calibration process and which also serve as a metric for evaluating the most appropriate model for the SOC estimation problem.

The combinations of forecasting models with optimization techniques, as well as the optimizer configuration parameters are defined. And finally, the basic concepts of the 4 driving test profiles used are presented in carrying out this study.

3. RESULTS

In this section, the results obtained in the training and testing of the models are presented. The training is obtained from the initial capacity curve, where the optimization techniques adjust the model coefficients in order to present the lowest sum of absolute error along the curve. Next, the results of the predictions obtained through the equations defined in the training process are presented.

3.1 MODEL TRAINING

3.1.1 TRAINING WITH GA

Figure 7 shows the best approximations obtained by GA for the three implemented models. It can be seen that POISSON-GA cannot approximate well, SPLINE-GA has difficulty representing curves near nodes, and GLM-GA gives large errors at the initial point and around 7000 s.

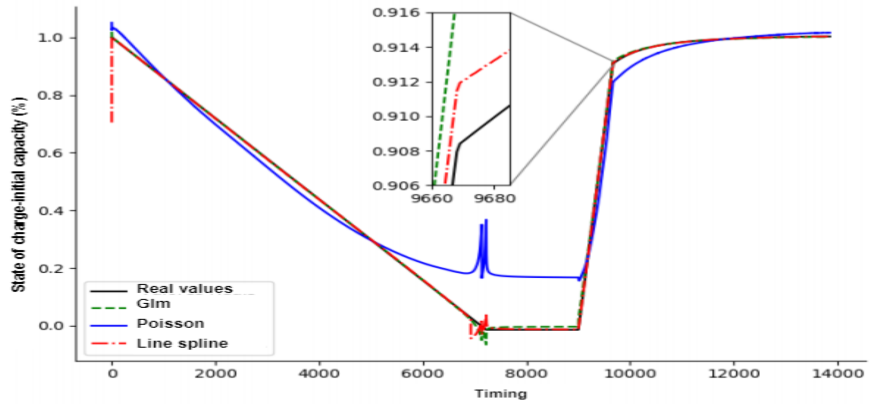

Figure 7 - GA training of the initial capacity curve

3.1.2 TRAINING WITH DE

Figure 8 presents the best approximation obtained through the DE for each of the three models. The approximation obtained through the POISSON-DE was not good, presenting a high error, the SPLINE-DE presented an error in the node points and finally, the GLM-DE presented an error in the range between 7000 and 9000 seconds.

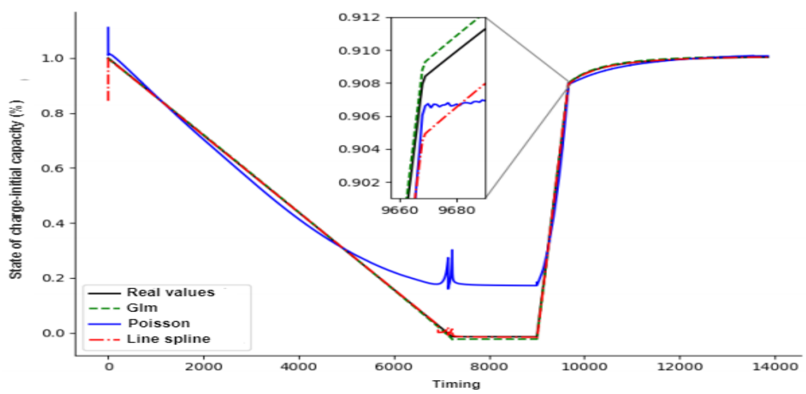

Figure 8 – ED training of the initial capacity curve

3.1.3 TRAINING WITH THE PSO

Figure 9 presents the best approximation obtained through the PSO for each of the three models. The approximation obtained through the POISSON-PSO presented error along the entire curve, the SPLINE-PSO and the GLM-PSO obtained a satisfactory performance, presenting practically no training error.

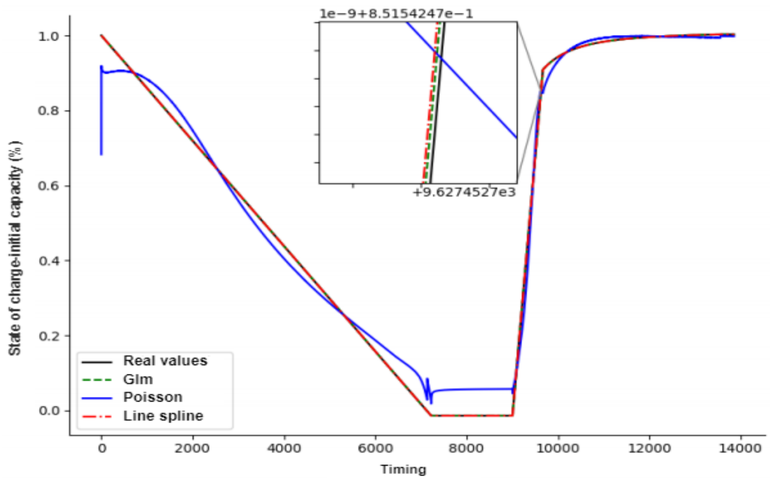

Figure 9 – Initial capacity curve PSO training.

3.1.4 ANALYSIS OF THE TRAINING

Figure 10 shows the scatter plot that was plotted from the fitness function. The closer to 1 the better the answer obtained. Each algorithm was executed 50 times, where it can be seen that the GLM-PSO obtained the best response.

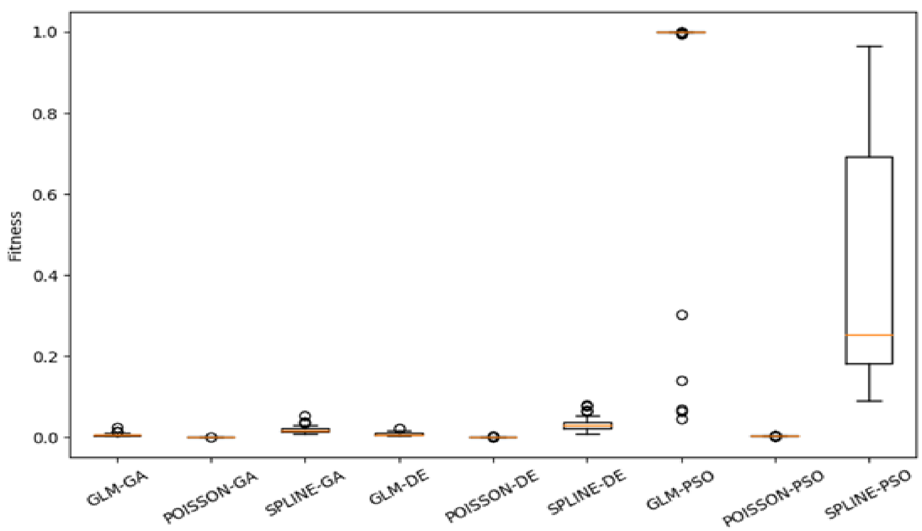

Figure 10 – Fitness dispersion graph for 50 runs

Figure 11 shows the scatter plot that was plotted from the cost function, which corresponds to the sum of the errors module along the entire curve. The closer to zero, the better the response obtained. Each algorithm was executed 50 times, where it can be seen that the GLM-PSO and SPLINE-PSO presented the best response.

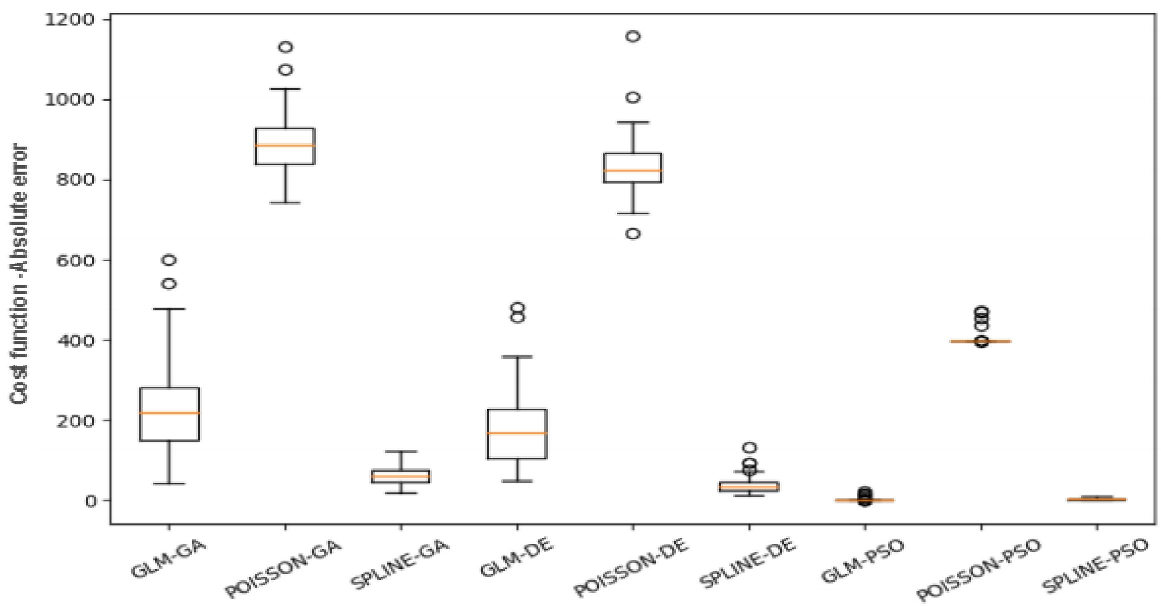

Figure 11 – Scatter plot function absolute error cost (AE) for 50 runs

Finally, Figure 12 shows the dispersion of convergence values for the 50 runs. For linear interpolation, the number of iterations used until convergence was added.

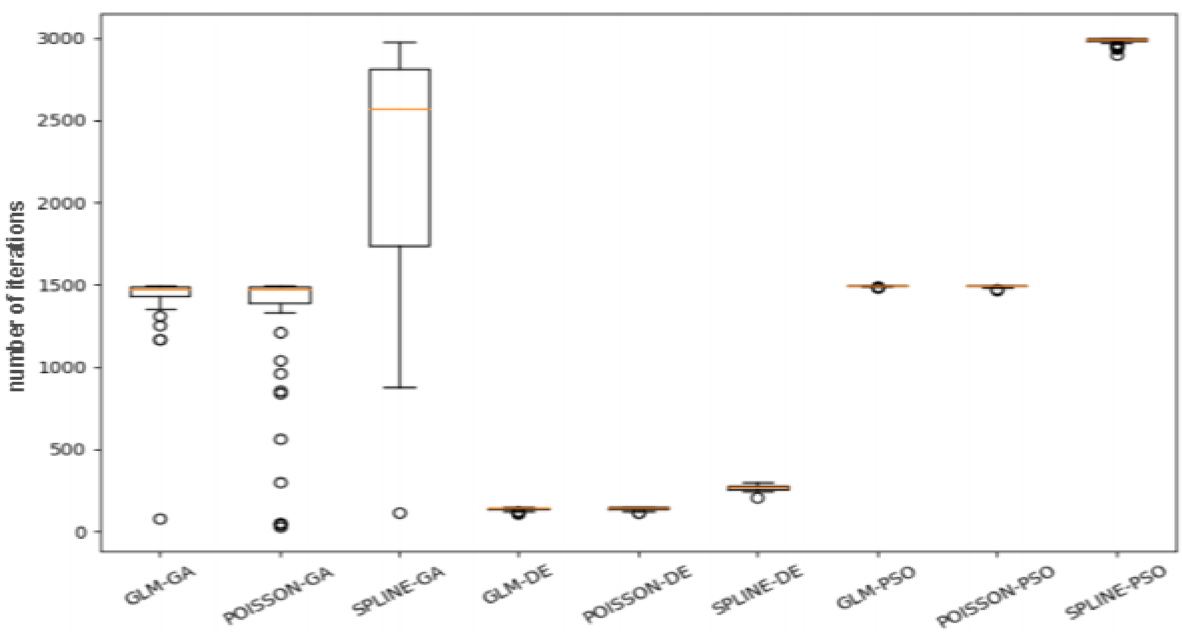

Figure 12 – Convergence scatter plot for 50 runs

Table 2 presents the best execution results obtained from the respective approximations of the initial capacity curve. The table shows the absolute error (AE), fitness and convergence generation, so that the GLM-PSO presented the best result. This superiority can be attributed to the characteristics of the GLM-PSO, which for this specific case made the absolute error close to zero.

Table 2 - Optimization results for the training algorithms

Model	AE	Fitness	Convergence Generation
I	42.120	0.01671	1433
II	740.726	0.00459	1473
III	21.516	0.03651	2741
IV	47.341	0.01431	135
V	663.209	0.00439	145
VI	13.534	0.05821	253
VII	1.065	0.99401	1496
VIII	396.175	0.00339	1491
IX	0.002	0.99301	2992

3.2 MODEL TESTING

Four test profiles were used in the validation process of the models trained from the initial capacity curve. The results obtained through these test profiles are presented below.

3.2.1 RESULTS OF THE DST TEST PROFILE

As previously mentioned, the tests take place in three controlled temperature ranges within the battery operating range, namely: 0ºC, 25ºC and 45ºC with the initial SOC at 50% and 80%. Tables 3-8 present the results obtained from the DST test profile, for the metrics AE, MAE and MSE, where the GLM-PSO was superior in all variations of SOC and temperature.

Table 3 - DST forecast results for 0º Celsius and 50% SOC

Model	AE	MAE	MSE
I	542.6777	0.095768	0.00251
II	398.4427	0.068823	3.097423
III	1299.013	0.23706	0.158781
IV	64.76353	0.006488	0.00588
V	394.508	0.068088	3.194133
VI	895.6519	0.161708	0.067925
VII	6.41E-06	1.21E-09	1.46E-18
VIII	67772.13	12.65498	4.663077
IX	838.7007	0.151069	0.09406

Table 4 - DST forecast results for 0º Celsius and 80% SOC

Model	AE	MAE	MSE
I	8691.434	0.928633	0.00251
II	4029.895	0.4275	19.19442
III	5247.868	0.558437	0.862121
IV	547.1701	0.053094	0.00588

V	4015.97	0.426003	18.73566
VI	5393.941	0.57414	1.194392
VII	1.49838	0.00589	0.00589
VIII	6.7E+21	7.21E+17	1632.441
IX	10072.46	1.077098	4.687797

Table 5 - DST forecast results for 25º Celsius and 50% SOC

Model	AE	MAE	MSE
I	52.27189	0.00428	0.00251
II	169.9934	0.026547	2.369946
III	1277.837	0.236087	0.154642
IV	11.4935	0.00343	0.00588
V	171.804	0.026889	2.267352
VI	707.5266	0.128217	0.042096
VII	1.49849	0.00589	0.00589
VIII	417.8476	0.073426	2.082866
IX	220.6499	0.036128	1.00251

Table 6 - DST forecast results for 25º Celsius and 80% SOC

Model	AE	MAE	MSE
I	8982.331	0.946594	0.00251
II	4063.114	0.425049	20.54458
III	5613.142	0.589386	0.976727
IV	530.9245	0.050559	0.00588
V	4041.142	0.422719	19.55547
VI	5607.33	0.58877	1.2527
VII	1.49838	0.00589	0.00589
VIII	3.14E+22	3.33E+18	1766.126
IX	10421.3	1.099156	1.00251

Table 7 - DST forecast results for 45º Celsius and 50% SOC

Model	AE	MAE	MSE
I	5041.292	0.933877	0.00251
II	1534.424	0.280342	21.4629
III	2920.651	0.538678	0.800442
IV	321.2501	0.054257	0.00588
V	1527.945	0.279135	20.73174
VI	3050.58	0.562891	1.190994

VII	1.49843	0.00589	0.00589
VIII	4E+21	7.46E+17	1661.357
IX	5695.321	1.055761	1.00251

Table 8 - DST forecast results for 45º Celsius and 80% SOC

Model	AE	MAE	MSE
I	437.1875	0.040724	0.00251
II	493.4039	0.046698	1.543525
III	2360.999	0.245146	0.177377
IV	26.1057	0.00296	0.00588
V	720.817	0.070862	1.480447
VI	1289.776	0.131319	0.052062
VII	1.49848	0.00589	0.00589
VIII	3621.257	0.379059	11.58072
IX	313.4639	0.027577	1.00251

3.2.2 RESULTS FROM THE FUDS TEST PROFILE

Tables 9-14 present the results obtained from the FUDS test profile, for the metrics AE, MAE and MSE, where the GLM-PSO was superior in all variations of SOC and temperature.

Table 9 - FUDS forecast results for 0º Celsius and 50% SOC

Model	AE	MAE	MSE
I	640.59	0.107154	0.00251
II	471.2753	0.077345	3.233667
III	1394.71	0.239921	0.163844
IV	73.67011	0.007344	0.00588
V	466.163	0.076445	3.335701
VI	929.3454	0.157991	0.074954
VII	1.49848	0.00589	0.00589
VIII	118663.5	20.88584	6.976529
IX	1061.01	0.181171	1.00251

Table 10 - FUDS forecast results for 0º Celsius and 80% SOC

Model	AE	MAE	MSE
I	900.1229	0.088978	0.00251
II	1065.602	0.106389	2.554204
III	2585.225	0.266282	0.203948
IV	96.03471	0.004372	0.00588
V	1065.381	0.106366	2.640707
VI	1691.609	0.172257	0.083864
VII	1.49848	0.00589	0.00589
VIII	153704.3	16.16686	4.71014
IX	1828.862	0.186698	1.00251

Table 11 - FUDS forecast results for 25º Celsius and 50% SOC

Model	AE	MAE	MSE
I	3140.262	0.552149	0.00251
II	1377.892	0.239117	11.52936
III	2416.662	0.423623	0.444757
IV	194.9857	0.02901	0.00588
V	1354.198	0.234909	10.99592
VI	2077.232	0.363334	0.496785
VII	1.49845	0.00589	0.00589
VIII	1.91E+14	3.39E+10	569.0179
IX	3748.028	0.660101	1.00251

Table 12 - FUDS forecast results for 25º Celsius and 80% SOC

Model	AE	MAE	MSE
I	143.6589	0.009027	0.00251
II	276.0139	0.022628	1.886425
III	2538.474	0.255129	0.190884
IV	21.40707	0.00354	0.00588
V	379.3146	0.033244	1.824386
VI	1408.062	0.138963	0.054499
VII	1.49849	0.00589	0.00589
VIII	1200.056	0.117587	2.726069
IX	845.5315	0.081154	1.00251

Table 13 - FUDS forecast results for 45º Celsius and 50% SOC

Model	AE	MAE	MSE

I	305.9357	0.04898	0.00251
II	341.3851	0.055306	1.890762
III	1233.494	0.214526	0.140767
IV	12.6427	-0.00337	0.00588
V	435.7851	0.072155	1.80202
VI	672.1478	0.11434	0.034663
VII	1.49848	0.00589	0.00589
VIII	1466.045	0.256031	15.61608
IX	140.3034	0.019418	1.00251

Table 14 - FUDS forecast results for 45º Celsius and 80% SOC

Model	AE	MAE	MSE
I	551.8162	0.051	0.00251
II	676.6942	0.06384	1.469343
III	2415.735	0.242643	0.177007
IV	31.7878	-0.00247	0.00588
V	894.7201	0.086257	1.413336
VI	1316.255	0.129598	0.048396
VII	1.49848	0.00589	0.00589
VIII	3953.251	0.400726	15.29611
IX	473.4618	0.042944	1.00251

3.2.3 RESULTS OF TEST PROFILE US06

Tables 15-20 present the results obtained from the US06 test profile, for the AE, MAE and MSE metrics, where the GLM-PSO was superior in all SOC and temp variations.

Table 15 - US06 forecast results for 0º Celsius and 50% SOC

Model	AE	MAE	MSE
I	404.0647	0.073121	0.00251
II	320.0231	0.056748	2.810343
III	1214.365	0.230982	0.135736
IV	50.94734	0.004327	0.00588
V	307.8844	0.054383	2.892337
VI	776.5432	0.145686	0.052721
VII	1.49848	0.00589	0.00589
VIII	23507.57	4.574097	1.512312
IX	612.0614	0.113642	1.00251

Table 16 - US06 forecast results for 0º Celsius and 80% SOC

Model	AE	MAE	MSE
I	421.4111	0.040866	0.00251
II	550.8803	0.05518	2.077026
III	2362.405	0.255459	0.175676
IV	56.34709	0.000505	0.00588
V	523.5948	0.052163	2.131703
VI	1476.901	0.157559	0.06273
VII	1.49848	0.00589	0.00589
VIII	15074.43	1.66088	0.254194
IX	877.2168	0.091259	1.00251

Table 17 - US06 forecast results for 25º Celsius and 50% SOC

Model	AE	MAE	MSE
I	131.7133	0.019871	0.00251
II	150.5816	0.02352	2.116931
III	1215.959	0.22955	0.132178
IV	7.584928	-0.00413	0.00588
V	239.343	0.040685	2.014165
VI	660.4418	0.12212	0.035156
VII	1.49849	0.00589	0.00589
VIII	964.1399	0.180851	6.562319
IX	68.98756	0.007741	1.00251

Table 18 - US06 forecast results for 25º Celsius and 80% SOC

Model	AE	MAE	MSE
I	109.5733	0.006333	0.00251
II	267.1122	0.02367	1.881698
III	2449.815	0.263871	0.182071
IV	15.80428	-0.00399	0.00588
V	318.4238	0.029317	1.790329
VI	1354.25	0.143306	0.053287
VII	1.49849	0.00589	0.00589
VIII	820.5495	0.084574	2.231158
IX	411.6076	0.039571	1.00251

Table 19 - US06 forecast results for 45º Celsius and 50% SOC

Model	AE	MAE	MSE
I	284.7444	0.050017	0.00251

II	305.0756	0.053988	1.852556
III	1163.049	0.221561	0.12487
IV	12.19141	0.00322	0.00588
V	395.6165	0.071672	1.743926
VI	635.7839	0.118579	0.033722
VII	1.49849	0.00589	0.00589
VIII	1377.417	0.263429	14.94779
IX	141.8533	0.022108	1.00251

Table 20 - US06 forecast results for 45º Celsius and 80% SOC

Model	AE	MAE	MSE
I	511.5743	0.050684	0.00251
II	615.6424	0.06216	1.468556
III	2306.008	0.248549	0.164509
IV	31.36514	0.00227	0.00588
V	829.6357	0.085756	1.384424
VI	1282.028	0.135639	0.050259
VII	-1.49848	0.00589	0.00589
VIII	3667.656	0.398692	14.00081
IX	214.6892	0.017948	1.00251

3.2.4 RESULTS OF THE BJDST TEST PROFILE

Tables 21-26 present the results obtained from the BJDST test profile.for the metrics AE, MAE and MSE, where the GLM-PSO was superior in all variations of SOC and temperature.

Table 21 - BJDST forecast results for 0º Celsius and 50% SOC

Model	AE	MAE	MSE
I	298.7255	0.04943	0.00251
II	281.1005	0.046183	2.589928
III	1227.578	0.220584	0.119955
IV	40.99608	0.00194	0.00588
V	260.1402	0.042321	2.613079
VI	777.0635	0.137571	0.043048
VII	1.49849	0.00589	0.00589
VIII	9650.339	1.772595	0.229389
IX	375.3955	0.063558	1.00251

Table 22 - BJDST forecast results for 0º Celsius and 80% SOC

Model	AE	MAE	MSE

I	727.0712	0.071363	0.00251
II	917.2386	0.091527	2.385788
III	2647.801	0.275024	0.202521
IV	65.11217	0.001173	0.00588
V	852.0408	0.084614	2.373336
VI	1696.067	0.174108	0.072071
VII	1.49848	0.00589	0.00589
VIII	94989.28	10.0663	3.141993
IX	921.0523	0.091931	1.00251

Table 23 - BJDST forecast results for 25º Celsius and 50% SOC

Model	AE	MAE	MSE
I	155.5451	0.023458	0.00251
II	167.8506	0.025758	2.08981
III	1197.868	0.218249	0.11653
IV	6.424782	-0.00441	0.00588
V	257.866	0.04258	1.957545
VI	654.4712	0.116698	0.031622
VII	1.49849	0.00589	0.00589
VIII	1053.325	0.191236	6.999294
IX	87.64577	0.010769	1.00251

Table 24 - BJDST forecast results for 25º Celsius and 80% SOC

Model	AE	MAE	MSE
I	293.3708	0.025093	0.00251
II	272.0841	0.022857	1.666281
III	2527.586	0.259854	0.17785
IV	20.73359	0.00355	0.00588
V	496.6261	0.046451	1.549264
VI	1408.712	0.142288	0.055115
VII	1.49849	0.00589	0.00589
VIII	2876.314	0.296497	6.284475
IX	128.9319	0.007815	1.00251

Table 25 - BJDST forecast results for 45º Celsius and 50% SOC

Model	AE	MAE	MSE
I	305.7566	0.051466	0.00251
II	321.7207	0.054446	1.853844

III	1163.607	0.211602	0.109572
IV	14.30907	-0.00294	0.00588
V	426.5761	0.074019	1.715721
VI	642.603	0.114345	0.030727
VII	4.17E-06	7.80E-10	6.20E-19
VIII	1427.623	0.260886	14.4825
IX	245.1422	0.040151	0.002612

Table 26 - BJDST forecast results for 45º Celsius and 80% SOC

Model	AE	MAE	MSE
I	549.9055	0.052491	0.00239
II	637.7175	0.061788	1.465597
III	2442.041	0.252822	0.168499
IV	36.60695	0.00186	0.00587
V	890.5083	0.088552	1.347168
VI	1377.086	0.140069	0.054819
VII	**6.60E-06**	**7.00E-10**	**5.24E-19**
VIII	3797.904	0.396376	13.3643
IX	400.5957	0.036682	0.001481

By analyzing the test profiles, it can be seen that the implemented algorithms obtained good results, especially the GLM-PSO, which was superior to the others in all tests and temperature conditions.

This section presented the results obtained in the training and testing process used in the SOC prediction process**.**

Among the three models used in training, it can be seen that POISSON was the one that had the greatest difficulty in representing the initial capacity curve. SPLINE and GLM were more accurate in this process.

For the calibration process, the GLM-PSO obtained the best performance, reaching close to zero. For this problem in particular, GA and DE have difficulty in fine-tuning, this difficulty does not rule out their use, as each of these algorithms has a huge number of variations, so that possibly local search operators could improve the performance of the same. However, it is clear that PSO performed better, achieving accurate calibration when added to GLM and SPLINE.

As POISSON did not perform satisfactorily in the training process, it did not obtain adequate predictions in the testing process. The results obtained by the SPLINE-PSO, even though they were satisfactory in the training process, were much lower than the GLM-PSO in the predictions, where the stretches and node points of the SPLINE presented greater error. In this way, among the nine combinations presented, the most suitable for the SOC prediction problem is the GLM model with 69 the PSO optimizer.

When compared to the work by [31] who obtained MAE close to 1% and 0.6% in their estimators, the GLM-PSO was superior, reaching MAE values close to zero.

4. CONCLUSIONS AND PERSPECTIVES

Predicting the SOC of the battery is a fundamental step for the new generation of EVs. This work carried out the training of the models through the initial capacity curve of an INR 18650-20R LiNiMnCoO2/Graphite battery. For testing and validation of the results, the forecast was used from 4 internationally recognized test profiles: DST, FUDS, US06 and BJDST. Altogether, they were the combinations of three models were implemented: GLM, POISSON and SPLINE with 3 different computational intelligence techniques: GA, DE and PSO, which resulted in nine combinations.

As a result, a specific algorithm was much superior to the others, so that the GLM-PSO practically did not show error in training, with a faithful representation of the initial capacity curve, as well as a high performance in all test profiles. This proposal presents superior performance to other more sophisticated techniques and models, such as SPLINE.

Finally, as future work, different battery models can be tested, as well as the application of more variations in computational intelligence techniques.

REFERENCES

1. M. Kia, M. Shafiekhani, H. Arasteh, S. Hashemi, M. Shafie-Khah, and J. Catalão, "Short-term operation of microgrids with thermal and electrical loads under different uncertainties using information gap decision theory," Energy, vol. 208, Article ID 118418, 2020.
2. Baghaee, H.R. Real-Time Verification of New Controller to Improve Small/Large-Signal Stability and Fault Ride-Through Capability of Multi-DER Microgrids. IET Gener. Transm. Distrib. 2016, 10, 3068–3084.
3. A. Akbari, V. Vahidinasab, H. Arasteh, and E. Kazemi-Robati, "Rural and residential microgrids: concepts, status quo, model, and application," in Residential Microgrids and Rural Electrifications, pp. 131–161, Elsevier, Netherlands, Europe, 2022.
4. Hirsch, A.; Parag, Y.; Guerrero, J. Microgrids: A Review of Technologies Key Drivers and Outstanding Issues. Renew. Sustain. Energy Rev. 2018, 90, 402–411.
5. R. S. Sankarkumar and R. Natarajan, "Energy management techniques and topologies suitable for hybrid energy storage system powered electric vehicles: an overview," International Transactions on Electrical Energy Systems, vol. 31, no. 4, Article ID 12819, 2021.
6. Farrokhabadi, M.; Cañizares, C.A.; Simpson-Porco, J.W.; Nasr, E.; Fan, L. Microgrid Stability Definitions, Analysis, and Examples. IEEE Trans. Power Syst. 2019, 35, 13–29.
7. Ullah, S.; Khan, L.; Jamil, M.; Jafar, M.; Mumtaz, S.; Ahmad, S. A Finite-Time Robust Distributed Cooperative Secondary Control Protocol for Droop-Based Islanded AC Microgrids. Energies 2021, 14, 2936.
8. N. Drir, F. Chekired, and D. Rekioua, "An integrated neural network for the dynamic domestic energy management of a solar house," International Transactions on Electrical Energy Systems, vol. 31, no. 12, Article ID 13227, 2021.
9. Moazeni, F.; Khazaei, J. Optimal Operation of Water-Energy Microgrids; A Mixed Integer Linear Programming Formulation. J. Clean. Prod. 2020, 275, 122776.
10. L. Yang, Q. Sun, D. Ma, and Q. Wei, "Nash Q-learning based equilibrium transfer for integrated energy management game with We-Energy," Neurocomputing, vol. 396, pp. 216–223, 2020.
11. Hannan, M. A. et al. A review of lithium-ion battery state of charge estimation and management system in electric vehicle applications: Challenges and recommendations. Renewable and Sustainable Energy Reviews, v. 78, p. 834–854, 2017.73
12. Hassan, M.K. et al. Optimal design of electric power assisted steering system (EPAS) using GA-PID method. Procedia Engineering, v. 41, p. 614–621, 2012.
13. He, H. et al. Online model-based estimation of state-of-charge and open-circuit voltage of lithium-ion batteries in electric vehicles. Sustainable Energy and Environmental Protection 2010, v. 39, n. 1, p. 310–318, 2012.
14. He, Y.; Liu, W.; Koch, B. J. Battery algorithm verification and development using hardware-in-the-loop testing. Journal of Power Sources, v. 195, n. 9, p. 2969–2974, 2010.
15. Holland, J. H. Genetic algorithms. Scientific American, v. 267, p. 66–73, 1992. HU, X. et al. Charging time and loss optimization for LiNMC and LiFePO4 batteries based on equivalent circuit models. Journal of Power Sources, v. 239, p. 449–457, 2013.
16. Hu, Y. Electro-thermal battery model identification for automotive applications. Journal of Power Sources, v. 196, n. 1, p. 449–457, 2011.
17. Hu, Y. et al. A technique for dynamic battery model identification in automotive applications using linear parameter varying structures. Control Engineering Practice, v. 17, n. 10, p. 1190–1201, 2009.
18. Martins, M.S.R. et al. Pso with path relinking for resource allocation using simulation optimization. Computers & Industrial Engineering, v. 65, n. 2, p. 322–330.
19. Mendes, J. et al. An architecture for adaptive fuzzy control in industrial environments. Computers in Industry, v. 62, n. 3, p. 364–373, 2011.
20. Tabar, V.S.; Ghassemzadeh, S.; Tohidi, S. Energy Management in Hybrid Microgrid with Considering Multiple Power Market and Real Time Demand Response. Energy 2019, 174, 10–21.

21. Nelder, J. A.; Wedderburn, R. W. M. Generalized linear models. Journal of the Royal Statistical Society: Series A (General), v. 135, n. 3, p. 370–384, 1972.
22. Neuhaus, J.; Mcculloch, C. Generalized linear models. Wiley Interdisciplinary Reviews: Computational Statistics, v. 3, n. 5, p. 407–413, 2011.75
23. Rahimi-Eichi, H. et al. Battery management system: An overview of its application in the smart grid and electric vehicles. IEEE Industrial Electronics Magazine, v. 7, n. 2, p. 4–16, 2013.
24. Rahman, M. A.; Anwar, S.; Izadian, A. Electrochemical model parameter identification of a lithium-ion battery using particle swarm optimization method. Journal of Power Sources, v. 307, p. 86–97, 2016.
25. Shafiekhani, A.; Mahjoob, M.J.; Akraminia, M. Design and implementation of an adaptive critic-based neuro-fuzzy controller on an unmanned bicycle Mechatronics, v. 28, p. 115–123, 2015.
26. Shareef, H.; Islam, M. M.; Mohamed, A. A review of the stage-of-the-art charging technologies, placement methodologies, and impacts of electric vehicles. Renewable and Sustainable Energy Reviews, v. 64, p. 403–420, 2016.
27. Y. Ji, J. Wang, J. Xu, X. Fang, and H. Zhang, "Real-time energy management of a microgrid using deep reinforcement learning," Energies, vol. 12, no. 12, p. 2291, 2019.
28. T. A. Nakabi and P. Toivanen, "Deep reinforcement learning for energy management in a microgrid with flexible demand," Sustainable Energy, Grids and Networks, vol. 25, Article ID 100413, 2021.
29. Yang, Z.; LI, K.; Foley, A. Computational scheduling methods for integrating plug-in electric vehicles with power systems: A review. Renewable and Sustainable Energy Reviews, v. 51, n. 4543, p. 396–416, 2015.
30. J. Jiang, S. Ji, and G. Long, "Decentralized knowledge acquisition for mobile internet applications," World Wide Web, vol. 23, no. 5, pp. 2653–2669, 2020.
31. Zheng, F et al. Influence of different open circuit voltage tests on state of charge online estimation for lithium-ion batteries. Applied Energy, v. 183, p. 513 – 525,2016.77
32. Öztürk, N.; Çelik, E. Speed control of permanent magnet synchronous motors using fuzzy controller based on genetic algorithms. International Journal of Electrical Power & Energy Systems, v. 43, p. 889–898, 2012.
33. Dhineshkumar, K., Amaleswari, R., & Prakash, G. (2026). A smart meter-integrated approach for optimizing EV charging infrastructure with enhanced sparrow search algorithm. Journal of the Chinese Institute of Engineers, 49(3), 624–638. https://doi.org/10.1080/02533839.2025.2567954.
34. S, Priya, Vinoth Kumar P, Sridevi V, M Batumalay, & Gunapriya D. "Convolutional Neural Network for Battery System Monitoring and SOC Estimation for Ev Applications to Achieve Sustainability." Journal of Applied Data Sciences [Online], 5.4 (2024): 1802-1813